Magnetite Nitrogen-Doped Carbon Quantum Dots from Empty Fruit Bunches for Tramadol Removal

Law Yong Ng [1,2,*], Amelia Kar Mun Chiang [1,2], Ching Yin Ng [3,*], Kai Joe Ng [1], Ebrahim Mahmoudi [4], Ying Pei Lim [5] and Muneer M. Ba-Abbad [6]

[1] Department of Chemical Engineering, Lee Kong Chian Faculty of Engineering and Science, Universiti Tunku Abdul Rahman, Kajang 43000, Selangor, Malaysia; ameliachiang@utar.edu.my (A.K.M.C.); kaijoe88@outlook.com (K.J.N.)

[2] Centre for Advanced and Sustainable Materials Research (CASMR), Universiti Tunku Abdul Rahman, Kajang 43000, Selangor, Malaysia

[3] Department of Chemical Engineering, Faculty of Engineering, Technology and Built Environment, Kuala Lumpur Campus, UCSI University, Kuala Lumpur 56000, Selangor, Malaysia

[4] Department of Chemical and Process Engineering, Faculty of Engineering and Built Environment, Universiti Kebangsaan Malaysia, Bangi 43600, Selangor, Malaysia; mahmoudi.ebi@ukm.edu.my

[5] School of Chemical Engineering, College of Engineering, Universiti Teknologi MARA, Shah Alam 40450, Selangor, Malaysia; yingpei@uitm.edu.my

[6] Gas Processing Center, College of Engineering, Qatar University, Doha P.O. Box 2713, Qatar; mbaabbad@qu.edu.qa

* Correspondence: lyng@utar.edu.my (L.Y.N.); ngcy@ucsiuniversity.edu.my (C.Y.N.)

Abstract: Tramadol is a widely used pain medication detected in wastewater treatment plants, prompting concerns about its impact on the environment and the effectiveness of wastewater treatment. Nitrogen-doped carbon quantum dots (NCQDs) can be used to remove pollutants from the contaminated water sources. However, NCQDs can hardly be recovered after applications, leading to high regeneration costs. Thus, this study aims to explore the use of magnetite nitrogen-doped carbon quantum dots (magnetite NCQDs) fabricated from empty fruit bunches (EFBs) to remove tramadol from wastewater treatment. Various analytical methods were conducted to characterize the magnetite NCQDs. Magnetite NCQDs showed excellent separation and aggregate-free properties. This study investigated the effect of the initial concentration of tramadol, the dosage of magnetite NCQD adsorbent, and the contact time while keeping other parameters constant. Tramadol was efficiently adsorbed within 40 min with an adsorption efficiency of over 85.9% and further photodegraded by 4.5% after being exposed to UV light after undergoing photocatalysis for 50 min. Magnetite NCQDs exhibited outstanding properties in removing tramadol after undergoing five cycles. This research provides a promising approach for developing a highly efficient adsorbent for treating tramadol-contaminated wastewater.

Keywords: magnetite nitrogen-doped carbon quantum dot; photocatalyst; fluorescent; adsorption; photocatalytic degradation; tramadol

1. Introduction

Pharmaceutical contaminants, notably tramadol, have become a major contributor to water pollution, posing a significant threat to aquatic life [1]. The escalating release of tramadol, a pain reliever with antidepressant and anxiolytic effects, into water bodies is primarily attributed to its widespread medical use, improper disposal of pharmaceuticals, and incomplete removal during wastewater treatment processes. This discharge adversely affects aquatic lives, leading to altered behavior and brain tissue damage, resulting in

diminished boldness and sociability. Even small amounts of pharmaceutical pollutants in wastewater present risks to both human health and aquatic ecosystems. There is an urgent need to develop a low-cost, efficient, and eco-friendly technique for removing pharmaceutical pollutants from wastewater, especially at low concentrations.

The advantageous properties of carbon as a support material are due to its chemical inertness, high electronic conductivity, large surface area, and unique pore architecture [2]. Carbon quantum dots (CQDs), a type of fluorescent nanomaterial, have attracted the interests of researchers due their stability, water solubility, low cost, and biocompatibility [3]. Nitrogen-doped carbon quantum dots (NCQDs) are specifically noted for their chemically modifiable amine and hydroxyl groups. By forming composite structures with Fe_2O_3 (magnetite), NCQDs modify the Fe_2O_3 surface by forming strong bonds that prevent aggregation, enhance stability, improve dispersibility, and facilitate electron transfer. NCQDs act as capping agents by attaching to the surface of magnetite nanoparticles, creating a protective layer that prevents particle agglomeration and oxidation, thereby enhancing the lifespan of the nanocomposite and improving its overall stability [4]. With quasi-spherical morphology and customizable photoluminescence, NCQDs are highlighted as excellent fluorescent nanomaterials, showing significant potential in various applications, including interacting with chemical pollutants in the environment.

Recognizing their abundance and their status as a natural source of carbon, this study focuses on using empty fruit bunches (EFBs) to produce nitrogen-doped carbon quantum dots (NCQDs) [5]. In Malaysia, where the palm oil industry generates approximately 95 million tons of EFBs annually, there is a growing interest in the valorization of the EFBs [6]. EFBs, composed of solid lignocellulosic wastes, contain various functional groups, making them a rich source of carbon, hydrogen, and oxygen [7]. EFBs can be used to produce NCQDs, potentially reducing waste production from the palm oil mill industry and contributing to a zero-waste discharge goal. Magnetite NCQDs could be used as adsorbents due to the presence of abundant functional groups such as hydroxyl, carboxyl, and amine groups on the NCQDs.

Adsorption is an effective and low-cost treatment for pharmaceutical pollutants, with a focus on nanoadsorbents. Magnetite nanocomposites produced from biomass can be highlighted as efficient and recyclable nanoadsorbents due to their magnetic and biocompatible properties, ease of tuning, functionalization, and ease of separation [8]. However, there is a need for surface modification of bare magnetite nanocomposites to prevent aggregation and oxidation, thus ensuring their optimal performance and their use for wider applications.

A two-step process is proposed in this study to remove tramadol. In the two-step process, an adsorption process is conducted, followed by photocatalysis utilizing light energy and a photocatalyst. Magnetite NCQDs are highlighted for their efficient light-trapping, charge carrier separation, and visible light absorption, making them a potential photocatalyst for tramadol degradation [9]. However, the potential recombination of electron/hole pairs is noted as a factor that could reduce photocatalytic efficiency. Thus, the current study evaluated the performance of tramadol removal from aqueous solution through adsorption and photocatalysis in a sequential manner.

2. Materials and Methods

2.1. Materials and Reagents

The raw material for lignin extraction, EFB fibers, was obtained from the Seri Ulu Langat Palm Oil Mill. Urea with 99% purity (Merck Sdn. Bhd., Kuala Lumpur, Malaysia) was used as the doping element in the fabrication of NCQDs. Hydrochloric acid (37–38%) and sodium hydroxide pellets (97%) (Merck Sdn. Bhd., Kuala Lumpur, Malaysia) were

used to extract lignin from EFBs. Tramadol (Duopharma (M) Sdn. Bhd., Kuala Lumpur, Malaysia), a common type of painkiller, was purchased and used to prepare the synthetic solution in this work. Iron (III) chloride hexahydrate (FeCl$_3$·6H$_2$O) with 99.9% purity (Merck Ltd., Mumbai, India) and iron (II) sulfate heptahydrate (FeSO$_4$·7H$_2$O) with 99.9% purity (Merck Ltd., Mumbai, India) were used to prepare the magnetite composites. The hydrothermal synthesis of NCQDs was conducted in a 100 mL Teflon-lined autoclave made of stainless steel. In addition to this, deionized water was used to prepare all aqueous solutions unless otherwise specified.

2.2. Pre-Treatment of EFBs and Synthesis of NCQDs

Based on the review of the existing research, lignin was identified as a suitable material for creating NCQDs due to its biocompatibility and biodegradability characteristics, using a hydrothermal method [9]. A mixture of 20 g of EFB fibers and a 10 wt% sodium hydroxide solution was heated at 150 °C for 2 h in an autoclave reactor. After cooling to room temperature, the mixture was filtered using filter paper (20–25 μm pore size) to separate the solid residue, leaving a black liquor [10]. The black liquor was left to stand for 12 h, after which its pH was adjusted to 3.0 using 2.0 M of hydrochloric acid.

The mixture was kept at room temperature for 24 h to precipitate the lignin. The precipitate was filtered using filter paper (20–25 μm pore size) and washed thoroughly with distilled water to remove residual chemicals. The resulting residue was dried in an oven at 70 °C for 24 h to produce dry lignin powder [11]. To synthesize NCQDs, the dry lignin powder was dissolved in deionized water and mixed with urea in a 1:4 molar ratio. The solution was transferred to a stainless-steel Teflon-lined autoclave reactor and heated at 180 °C for 8 h. After cooling to room temperature, the resulting dark brown substance was filtered using filter paper. NCQDs were synthesized in the presence of urea, while carbon quantum dots (CQDs) were produced using the same procedure but without urea. Finally, the liquid NCQDs were freeze-dried for 24 h to yield powdered NCQDs, as depicted in Figure 1.
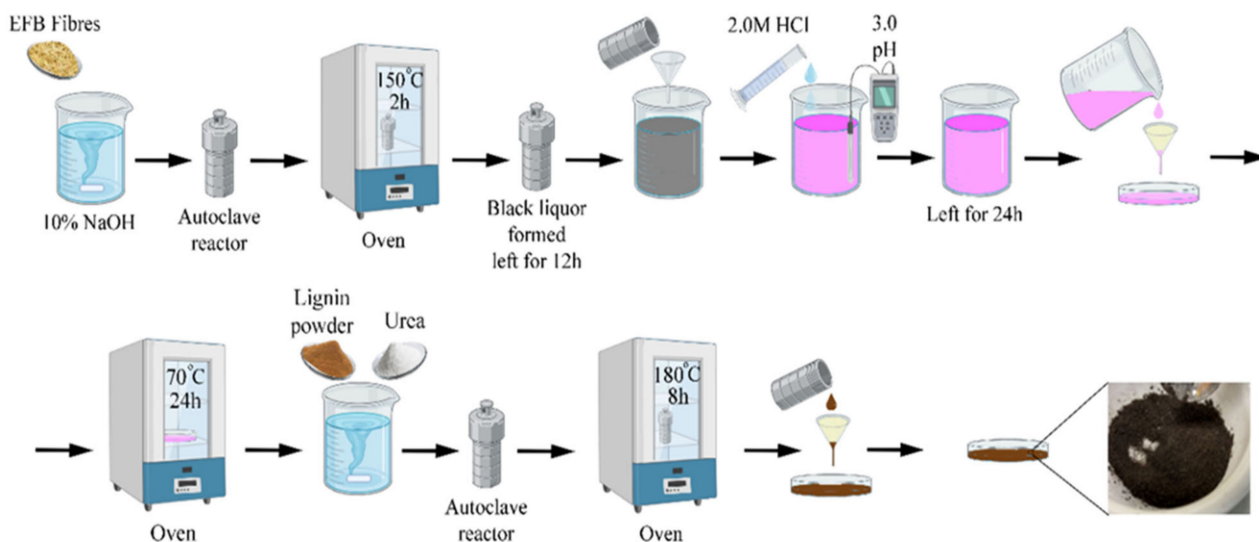

Figure 1. Fabrication process to produce NCQDs in powder form.

2.3. Synthesis of Magnetite NCQDs

A co-precipitation method was used to produce magnetite NCQDs by adding 1.1127 g of FeCl$_3$.6H$_2$O and 0.5708 g of FeSO$_4$.7H$_2$O to 100 mL of distilled water [4]. The process, depicted in Figure 2, was carried out in a 250 mL three-neck round-bottom flask, which was filled with an aqueous solution containing a 2:1 molar ratio of FeCl$_3$.6H$_2$O and FeSO$_4$.7H$_2$O

and stirred continuously for one hour at 80 °C under a nitrogen atmosphere to initiate the reaction. An inert nitrogen atmosphere is necessary to prevent the oxidation of ferrous ions (Fe^{2+}) to ferric ions (Fe^{3+}) by oxygen, thus ensuring that the reaction maintains a proper redox balance. The synthesis of magnetite NCQDs was carried out using Fe^{2+} and Fe^{3+} salts in a 1:2 molar ratio to facilitate the co-precipitation reaction necessary for the formation of Fe_3O_4. The presence of Fe^{3+} is critical for achieving the stoichiometric composition of magnetite and preventing the formation of other undesired iron oxide phases. This approach ensures the successful synthesis of magnetite NCQDs with the desired magnetic and structural properties.

Figure 2. Fabrication process to obtain magnetite NCQDs in powder form.

After one hour of stirring, a 25 mL solution of 10 mg/mL of diluted NCQDs was added to the flask, and the reaction continued for 30 min. Then, 20 mL of 2M NaOH was gradually added dropwise to the solution to enhance mixing, resulting in the formation of a black precipitate. The reaction was allowed to stir for an additional 2 h until the black precipitate was fully formed. External magnets (permanent magnets) were used to separate the black precipitate from the mixture through decantation. Finally, the black precipitates were washed with deionized water and dried at room temperature under vacuum conditions. The process flow to produce magnetite NCQDs in powder form is shown in Figure 2.

2.4. Characterization of CQDs, NCQDs, and Magnetite NCQDs

The properties of CQDs, NCQDs, and magnetite NCQDs produced through hydrothermal reaction from EFBs were evaluated. Various characterization techniques and instruments were used to investigate their functional groups, atomic percentage, fluorescent and optical properties, surface morphology, particle size distribution, electrostatic repulsion strength, and magnetic property.

Fourier Transform Infrared Spectroscopy (FTIR) (Nicolet iS10, Thermo Fisher Scientific, Waltham, MA, USA) was employed to examine the functional groups and energy dispersive X-ray (EDX) spectroscopy (Hitachi S-3400 N, Hitachi High Technologies America, Inc., Tokyo, Japan) was used to determine the atomic percentage of all samples. Photoluminescence spectroscopy (PL) (model Edinburgh Instrument FLS920, Edinburgh Instruments, Livingston, UK) and UV–Vis spectrophotometry (UV-2600, Shimadzu, Kyoto, Japan) were used to analyze the fluorescent and optical properties of all samples. Transmission electron microscopy (TEM) (Thermo Fisher, Waltham, MA, USA; Talos 120 C) was employed to

determine the particle size distribution of NCQDs and magnetic NCQDs. The particle size was further analyzed using ImageJ software Version 1.54m (National Institutes of Health, Bethesda, MD, USA; https://imagej.net/ij/index.html, accessed on 7 December 2024) to ensure accurate and consistent measurements. Finally, a zeta potential analysis was performed to examine the surface charges of the samples. The zeta potential of the NCQDs was measured using a Zetasizer Nano ZS (Malvern Instruments, Malvern, UK) in distilled water at a solution pH of 6.5 to determine the surface charges of the nanoparticles.

The magnetic properties of the magnetite NCQDs were evaluated using a vibrating sample magnetometer (VSM). Thermogravimetric analysis (TGA) and Differential Thermal Analysis (DTA) (using a Shimadzu DTG-60H Thermal Analyzer, Kyoto, Japan) were employed to assess the thermal properties of magnetite NCQDs. Thermal measurements were performed under the flow of nitrogen atmosphere with a flow rate of 100 mL min^{-1} in the temperature range of ambient to 250 °C. The heating rate was 20 °C per minute.

2.5. Adsorption of Tramadol

The adsorption experiments were conducted to evaluate the performance of magnetite NCQDs for the removal of tramadol. A stock solution of tramadol was prepared with initial concentrations ranging from 2 to 10 mg/L. Adsorbent doses varying from 0.01 g to 0.1 g were tested, and the contact time was investigated over a range of 0 to 60 min. The adsorption process was initially carried out to determine the optimal contact time, followed by assessments of the adsorbent dosage and the initial concentration of tramadol in the solution.

To evaluate the effectiveness of magnetite NCQDs in adsorbing tramadol from a tramadol solution (100 mL), standard batch adsorption experiments were conducted in 250 mL covered conical flasks under continuous stirring, and the results are presented as the average of data from three replicates. The study investigated several variables, including the initial tramadol concentration, the magnetite NCQD dosage, and the contact time, while keeping all other parameters constant. Kinetic experiments were performed using a selected dosage, and the tramadol solution concentrations were measured at fixed time intervals. After the specified adsorption period, an external magnet was used to separate the adsorbent from the solution. The remaining tramadol concentration was determined using a UV-Vis spectrophotometer at a wavelength of 271 nm, corresponding to its maximum absorption peak. This wavelength was chosen to ensure optimal sensitivity and accuracy in quantifying the tramadol concentration during the adsorption process. Tramadol uptake and the adsorption percentage were calculated using Equations (1) and (2), respectively.

$$Q_e = (C_o - C_e) \times V/m \tag{1}$$

$$Absorption \ (\%) = [(C_o - C_e)]/C_o \times 100 \tag{2}$$

where Q_e is the amount of solute adsorbed per unit mass of adsorbent at equilibrium (mg/g), C_o is the initial concentration of the solute in solution (mg/L), C_e is the equilibrium concentration of the solute in solution (mg/L), V is the volume of the solution (L), and m is the mass of the adsorbent (g).

Two adsorption kinetics models, namely the pseudo-first-order model and the pseudo-second-order model [12], were used to investigate the adsorption kinetics. A linearized mathematical form of the pseudo-first-order model is shown in Equation (3):

$$\log(Q_e - Q_t) = \log Q_e - \frac{k_1}{2.303} \times t \tag{3}$$

where k_1 is the pseudo-first-order rate constant (min^{-1}), t is the time (min), and Q_t is the amount of adsorbate on the adsorbent surface at time t (mg/g).

The linearized mathematical form of the pseudo-second-order model is shown in Equation (4).

$$\frac{t}{Q_t} = \frac{1}{h} + \frac{t}{Q_e}$$ (4)

where h is the initial adsorption rate ($h = k_2 Q_e{}^2$), k_2 is the overall pseudo-second-order rate constant, Q_e is the amount of adsorbate adsorbed at equilibrium (mg/g), and Q_t is the amount of adsorbate adsorbed at time t (mg/g).

2.6. Photocatalytic Degradation of Tramadol

This study evaluated the photocatalytic degradation efficiency of magnetite NCQDs on tramadol under a UV lamp (UVP Pen-Ray Lamp 11SC-1, UVP LLC, Upland, CA, USA) emitting at a wavelength of 365 nm, and the results are presented as the average of the data from three replicates. The UV lamp with a wavelength of 365 nm was selected for this study because tramadol molecules remain stable when exposed to UV-A irradiation in the absence of a photocatalyst [13]. The photocatalytic degradation process was conducted after the adsorption process in a polystyrene box with an orbital shaker, varying the photocatalysis contact time. A UV-Vis spectrophotometer was used to analyze the degraded tramadol solutions by measuring absorbance values at 271 nm. The degradation percentage of the tramadol solutions was calculated using Equation (5).

$$Degradation\ (\%) = [(A_o - A_t)/A_o]$$ (5)

where A_o is the initial concentration of tramadol solution and A_t is the concentration of tramadol solution after a specific time. Additionally, photocatalysis experiments were carried out to estimate the photodegradation kinetics rates using first-order and second-order kinetics models, represented by Equations (4) and (5), respectively. The rate constant k was determined from the slope of the graph. To further understand the reaction kinetics, the first-order kinetic model Equation (6) [14] was employed, shown as follows:

$$ln\ (A_o/A_t) = kt$$ (6)

where k is the first-order rate constant, calculated as the slope of the linear plot of $ln\ (A_0/A_t)$ versus time t. The data were also analyzed with a second-order kinetic model displayed by Equation (7) [15], which assumes a reaction rate proportional to the square of the reactant concentration. For this model, the rate constant k was determined from the slope of the linear plot of $1/A_t$ against time t.

$$\frac{1}{A_t} = kt + \frac{1}{A_0}$$ (7)

After the completion of the photodegradation process the photocatalyst could be isolated from the degraded tramadol by using an external magnet and reused in subsequent cycles.

2.7. Recyclability Study of the Magnetite NCQDs

The recyclability of the magnetite NCQDs was evaluated by conducting the adsorption process using 100 mL of tramadol solution at a concentration of 10 mg/L under dark conditions in a covered conical flask with continuous stirring at 200 rpm. The evaluation was conducted with 40 min of adsorption using 0.05 g of magnetite NCQDs, followed by 50 min of photocatalysis under a UV lamp with a wavelength of 365 nm. The magnetite NCQDs were separated from the tramadol solution using an external magnet, and the tramadol concentration was analyzed using a UV-Vis spectrophotometer at a wavelength of 271 nm.

The magnetite NCQDs were desorbed in a 0.1 M HCl solution with stirring at 200 rpm for an hour. The NCQDs were then filtered using a 0.45-micron filter paper, rinsed with distilled water, and dried in an oven overnight before being used for the next cycle. The recyclability test was repeated until the tramadol removal efficiency dropped below 80%.

3. Results and Discussion

3.1. Results of Functional Group Analyses

Figure 3 presents the FTIR spectra of CQDs, NCQDs, and magnetite NCQDs, highlighting the distinct structural differences between the samples. The FTIR spectrum of CQDs shows a prominent peak at 1608.8 cm^{-1}, attributed to C=C stretching vibrations, indicating the presence of aromatic rings due to the sp^2 hybridization of carbon atoms. The peak at 1039.2 cm^{-1} corresponds to ether (C–O–C) linkages, formed during the synthesis process. These peaks confirm the carbon-based structure of CQDs.
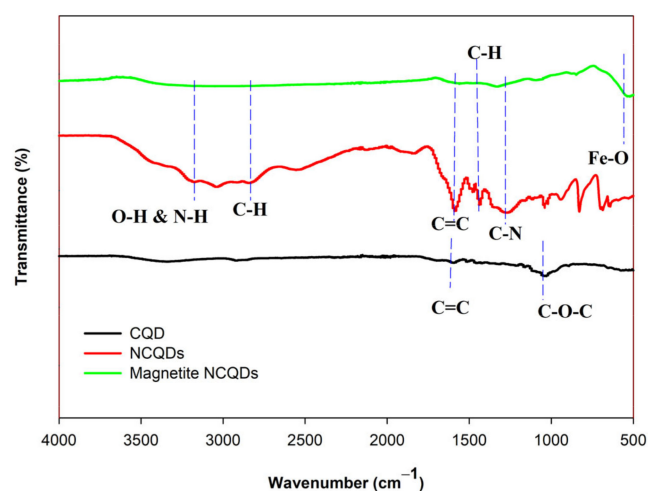

Figure 3. FTIR spectra of CQDs, NCQDs, and magnetite NCQDs.

In the NCQD spectrum, a broad peak between 3100 and 3542 cm^{-1} is observed, corresponding to −OH and −NH stretching vibrations. This indicates the presence of hydroxyl and amino groups on the surface of NCQDs. Aromatic −CH stretching and bending vibrations are observed at 2826.1 cm^{-1} and 1447.8 cm^{-1}, respectively. A strong absorption band at 1287.5 cm^{-1} corresponds to the −C=N− stretching frequency, which is formed through the condensation of primary amine groups during the nitrogen doping process. These peaks confirm the successful incorporation of nitrogen and the surface functionalization of NCQDs.

In the NCQD spectrum, a broad peak in the range of 3100–3542 cm^{-1} is attributed to the stretching vibrations of −OH and −NH groups, indicating the presence of multiple hydroxyl and amino groups on the NCQDs' surface. Aromatic −CH stretching vibrations and -CH bending vibrations are observed at 2826.1 cm^{-1} and 1447.8 cm^{-1}, respectively. Strong absorption bands at 1287.5 cm^{-1} are assigned to the −C=N− stretching frequency, which would be formed from the condensation of primary amine groups in NCQDs. However, in the magnetite NCQD spectrum, a peak at approximately 551 cm^{-1} indicates the presence of Fe–O stretching vibrations, characteristic of magnetite (Fe$_3$O$_4$). This band is attributed to the intrinsic Fe–O stretching vibrations within the magnetite structure.

The FTIR spectrum of magnetite NCQDs shows a characteristic peak at approximately 551 cm^{-1}, attributed to Fe–O stretching vibrations, confirming the presence of magnetite (Fe$_3$O$_4$). The addition of magnetite leads to a reduction in the intensity of carbon-based functional group peaks, such as those corresponding to −OH and −NH stretching vibra-

tions (3100–3542 cm^{-1}) and −C=N− (1287.5 cm^{-1}). This reduction is due to the partial surface coverage of NCQDs by magnetite, which limits the exposure of these functional groups and, consequently, their signal intensity in the FTIR spectrum.

The changes in FTIR peaks among CQDs, NCQDs, and magnetite NCQDs reflect the chemical modifications during synthesis. New peaks, such as −C=N and Fe–O, emerge due to nitrogen doping and magnetite incorporation, respectively. The reduction of peaks, such as −OH and −NH, further confirms the successful surface modification and formation of magnetite NCQDs.

3.2. Results of Elemental Composition Analyses

Table 1 displays the outcomes of the EDX analysis performed on CQDs, NCQDs, and magnetite NCQDs. The EDX study indicated that the primary components of the CQDs and NCQDs were carbon and oxygen. These components were believed to result from the presence of functional groups, such as hydroxyl, carbonyl, and aromatic rings. The existence of nitrogen in the NCQDs confirmed the successful incorporation of nitrogen into the structure of the quantum dots. The EDX analysis also revealed small traces of sodium and chlorine, which may have been caused by residual matter from the lignin preparation process. Nonetheless, the amount was insignificant and would not significantly impact the surface qualities of the quantum dots. Based on previous work, the composition percentages of nitrogen and oxygen were much lower than those found in the current research, which were 9.01 wt% and 20.38 wt%, respectively [9]. In that study, the researchers utilized oil palm empty fruit bunch fibers as the primary material. These fibers were subjected to an alkaline pre-treatment using sodium hydroxide to modify their structural and morphological properties for composite production. This may result from the choice of nitrogen- and oxygen-rich precursor materials, which likely led to higher nitrogen and oxygen percentages in the NCQDs in the current research.

Table 1. Elemental composition of CQDs, NCQDs, and magnetite NCQDs.

Element	Weight Percentage of CQDs (wt.%)	Weight Percentage of NCQDs (wt.%)	Weight of Percentage of Magnetite NCQDs (wt.%)
Carbon (C)	50.39	30.41	4.94
Nitrogen (N)	-	13.47	0.89
Oxygen (O)	34.62	34.70	25.44
Sodium (Na)	6.84	9.04	23.03
Chlorine (Cl)	8.15	12.37	-
Iron (Fe)	-	-	45.70

The successful formation of magnetite NCQDs is confirmed by the identification of iron (Fe), oxygen (O), carbon (C), and nitrogen (N) in the EDX data. In comparison to other studies, the weight percentage of oxygen was found to be 21.56 wt%. The current work showed a higher content of oxygen (25.44 wt.%), which is higher than a previous report of 21.56 wt% [16]. The higher oxygen content in this study indicates greater oxidation on the magnetite NCQDs' surface. The higher oxygen content may indicate increased oxidation on the magnetite NCQDs' surface, forming more oxygen-containing functional groups due to oxygen-rich precursors or synthesis conditions. The formation of NCQDs and magnetite NCQDs was confirmed using EDX analysis, identifying key elements, such as carbon, oxygen, nitrogen, and iron, consistent with QD structures. For future studies, high-resolution transmission electron microscopy (HRTEM) could be suggested to improve the resolution of the sample images, in addition to conducting EDX mapping to examine the elemental distribution and composition of the samples [17].

3.3. Results of Fluorescent Emission Analyses

To analyze the movement and recombination process of electron–hole pairs, PL was used to assess the fluorescent properties of CQDs, NCQDs, and magnetite NCQDs. Based on Figure 4, the excitation wavelength for CQDs was found to be 435 nm, while that for NCQDs was 433 nm. These luminescent characteristics may be due to the presence of abundant trap states resulting from sp^2 hybridization of carbon clusters and minor variations in the quantum dots' size distribution.
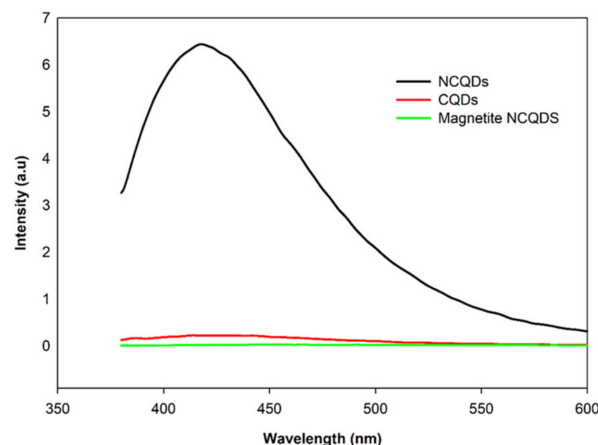
Figure 4. PL spectra of CQDs, NCQDs, and magnetite NCQDs.

The fluorescence characteristics of both CQDs and NCQDs are due to bandgap transitions that correspond to the conjugated π domain and surface defects present in them. However, NCQDs have a much higher excitation intensity compared to CQDs, which is reflected in their emission of higher energy. This difference may be due to the surface passivation functionality provided by nitrogen atoms. The lone pairs from nitrogen atoms have created new electronic transitions in NCQDs, resulting in increased photoluminescence intensity [18].

In its bulk form, magnetite NCQD exhibited low photoluminescent emission due to the local d-band's transitional nature. The magnetite NCQDs display a weak emission when excited at 450 nm radiation. The intense nature of the emission band indicates that the emission at around 450 nm corresponds to band edge emission, which is likely associated with the optical absorption at around 440 nm. The proposed structural model of hematite by Pauling and Hendricks suggests that there are changes in the oxygen atomic coordinates and an increase in Fe-O bonding separation in nanosized α-Fe_2O_3 [19]. This results in an enhancement of magnetic coupling between neighboring Fe^{3+} ions, which is responsible for the observed photoluminescence. However, the low PL properties could lead to the weak photocatalytic effect of the magnetite NCOQDs produced in this study.

3.4. Results of Optical Analyses

Figure 5 depicts the UV-Vis spectra of the samples. The spectra show an absorption band in the UV region for both CQDs and NCQDs, which is attributed to the absorption of the aromatic π system or the n-π* transition of carbonyl groups. For CQDs, the absorption peak at around 275 nm is due to the π-π* transition of the C=C bond, whereas NCQDs exhibit two small peaks at around 275 nm and 350 nm, originating from the aromatic π system and the n-π* transition of the C=O/C=N bond, respectively. The presence of amino groups in NCQDs causes the red-shifted absorption peaks. The addition of auxochromes to CQDs shifts the absorption peaks to longer wavelengths and changes their intensity. Nitrogen groups with unshared electron pairs can react with CQDs. C=C bonds, absorbing at 250–280 nm, and C=N or C=O bonds, absorbing around 343 nm, are involved in forming NCQDs.
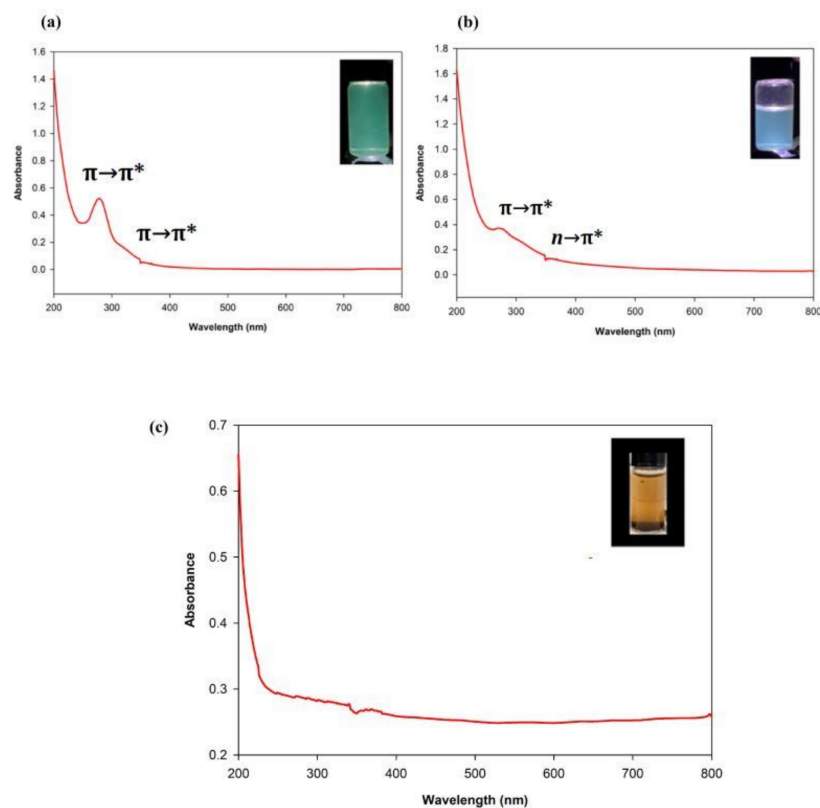
Figure 5. UV-Vis spectra of (**a**) CQDs (with the emission appearance shown in the inset on the right), (**b**) NCQDs (with the emission appearance shown in the inset on the right), and (**c**) magnetite NCQDs (with the emission appearance shown in the inset on the right).

Furthermore, when exposed to UV light at 360 nm, water-soluble CQDs and NCQDs emit bright green and blue fluorescence, respectively, as shown in the insets of Figure 5. The UV light source used for 360 nm excitation was a UVP Pen-Ray Lamp 11SC-1 (4 W, UVP LLC). Samples were diluted to 0.01 mg/mL in deionized water to ensure uniform dispersion. Fluorescence emission was measured using an Edinburgh Instruments FLS920 spectrometer. The 360 nm excitation wavelength was chosen based on characteristic absorption peaks, with additional tests at other wavelengths confirming optimal fluorescence detection at this wavelength.

The photo absorption and fluorescence emission results are linked through electronic transitions in CQDs and NCQDs. UV-Vis absorption peaks correspond to π-π* and n-π* transitions, indicating the ability to absorb light energy, which is emitted as fluorescence upon relaxation of excited electrons. The observed green and blue fluorescence aligns with the absorption characteristics, confirming the unique optical properties of the quantum dots. This demonstrates that CQDs and NCQDs possess distinctive UV absorption and fluorescence emission properties. The fluorescence emitted by CQDs and NCQDs aligns with a previous study, where similar samples exhibited pale blue and blue fluorescence, respectively [20].

Figure 5 presents the UV-Vis absorption spectra for magnetite NCQDs, with a strong absorption peak at around 200 nm, which is associated with the π-π* transition in the NCQDs. This could suggest that the integration of magnetite nanocomposites and NCQDs was successful. Coincidently, a similar observation was reported in another study that produced magnetite NCQDs using lemon juice as the raw material [4].

3.5. Results of Particles Size Analyses

Figure 6a–c demonstrate the TEM images of CQDs, NCQDs, and magnetite NCQDs. Figure 6d–f show the CQDs', NCQDs', and magnetite NCQDs' size distributions. The CQDs, NCQDs, and magnetite NCQDs are evenly dispersed and have a consistent shape. About 100 particles were analyzed to determine their average diameter. The size distributions of the CQDs, NCQDs, and magnetite NCQDs were plotted as Gaussian curves with a 95% confidence interval. The average particle size of the CQDs was determined to be approximately 4.78 nm, with a narrow size distribution, indicating consistent and uniform synthesis conditions. For NCQDs, the particle size showed a slightly broader distribution, with an average size of 5.87 nm, attributed to the inclusion of nitrogen dopants, which can alter the particle formation dynamics. Meanwhile, magnetite NCQDs exhibited the largest average particle size, around 13.53 nm, likely due to the influence of multi-dopant incorporation during the synthesis. The size distribution for all samples was predominantly within the nanoscale range, confirming the successful fabrication of quantum dots suitable for their application.
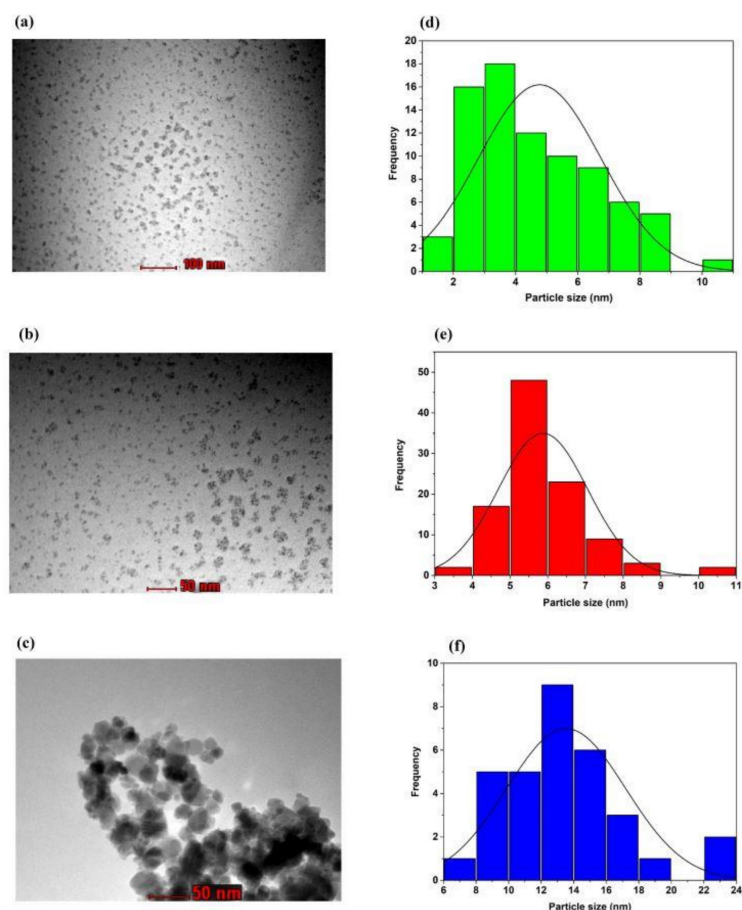

Figure 6. TEM images of (**a**) CQDs, (**b**) NCQDs, and (**c**) magnetite NCQDs in addition to the size distributions of (**d**) CQDs, (**e**) NCQDs, and (**f**) MNCQDs.

3.6. Results of Zeta Potential Analyses

Nanocomposites possess surface charges that cause them to interact with each other electrostatically. The zeta potential analysis can be used to determine the strength of this interaction. The zeta potential analysis showed that both CQDs and NCQDs had electrostatic charges at a solution pH of 6.5, with values of -16.70 ± 10.6 mV and -26.2 ± 8.64 mV, respectively, as shown in Figure 7a,b. The negative charge exhibited by both types of quantum dots implies the existence of negatively charged functional groups (such as OH

and COOH) on their surfaces. As these negatively charged quantum dots possess an excess of electrons, they are ideal for the photocatalytic degradation of organic pollutants as they can interact with electron-deficient species. To maintain a stable suspension in an aqueous solution, it is necessary to have oxygenated functional groups on the surfaces of both CQDs and NCQDs. Moreover, the similar charges on the surfaces of CQDs and NCQDs create a repulsive Coulombic force that prevents agglomeration and supports stable water dispersion of the products.
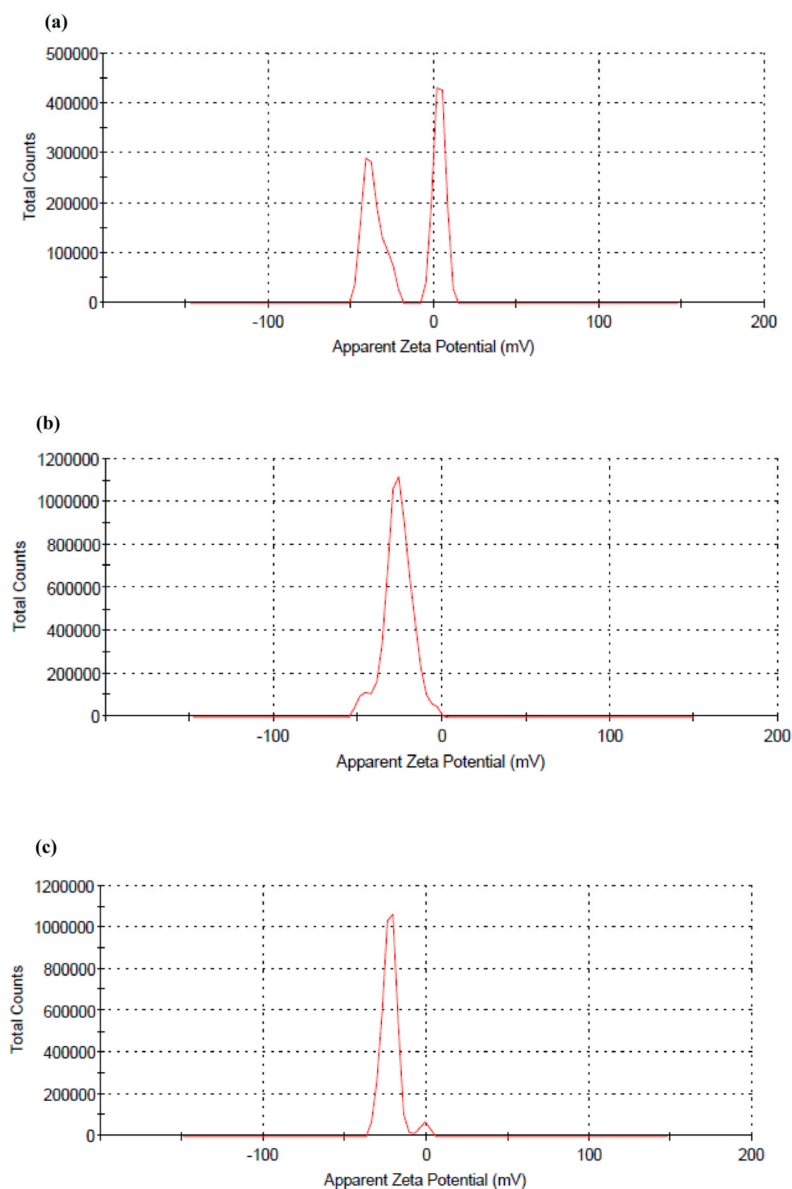
(a)

(b)

(c)

Figure 7. Zeta potential distribution of (**a**) CQDs, (**b**) NCQDs, and (**c**) magnetite NCQDs.

The zeta potential results in Figure 7c indicate that the magnetite NCQDs have a zeta potential of -22.0 ± 6.06 mV. This negative charge density is attributed to the presence of carboxylic acid groups on the surface. The slightly weaker zeta potential compared to NCQDs (-26.2 ± 8.64 mV) is likely due to surface chemistry changes caused by magnetite's incorporation [21]. The ability of the prepared magnetite nanocomposites to disperse and remain stable was evaluated by measuring their zeta potential. It is widely recognized that nanocomposites that have a higher charge and a smaller size distribution are less likely to aggregate. The negative charge density of the precursor NCQDs is attributed to the presence of carboxylic acid groups on their surface. This negative charge helps prevent

aggregation by producing repulsive forces between adjacent molecules, thereby contributing to the stability of the precursor NCQDs. The incorporation of magnetite alters the surface chemistry, further influencing the stability and charge of the final nanocomposites. Despite this partial surface coverage, the zeta potential analysis shows that magnetite NCQDs exhibit a slightly weaker zeta potential (-22.0 ± 6.06 mV) compared to NCQDs (-26.2 ± 8.64 mV). This could be attributed to residual carboxylic acid groups on the NCQDs' surface after magnetite incorporation. These groups contribute to the overall negative charge but with slightly lower charge density due to surface modifications caused by the magnetite.

3.7. Results of Thermogravimetric and Differential Thermal (TGA-DTA) Analyses

The TGA-DTA analysis of magnetite NCQDs is presented in Figure 8. The analysis revealed three stages of decomposition. The first stage resulted in a weight loss of around 15.0%, attributed to the loss of water. The second stage caused a weight loss of approximately 18.2%, corresponding to the decomposition of amine, hydroxyl, and carbonyl groups on the surface of the NCQDs within the nanocomposite structure. In addition to the TGA curve, Figure 8 also shows the DTA curve, which revealed three peaks. The first peak, occurring in the temperature range of 39–150 °C with a maximum at 80.14 °C, corresponds to the first-stage transition, possibly due to water loss. The second peak, occurring in the temperature range of 150–405 °C with a maximum at 274.33 °C, corresponds to the second-stage transition and is attributed to the decomposition of amine, hydroxyl, and carbonyl groups on the surface of the carbon quantum dots. The third peak, occurring in the temperature range of 404–735 °C with a maximum at 449 °C, corresponds to the third-stage transition and due to the structural rearrangement of the magnetite NCQDs. The results demonstrated the stability of the magnetite NCQDs compared to previous work, as less than 20% weight loss was observed, and all three peaks of the magnetite NCQDs' transitions were completed [22].
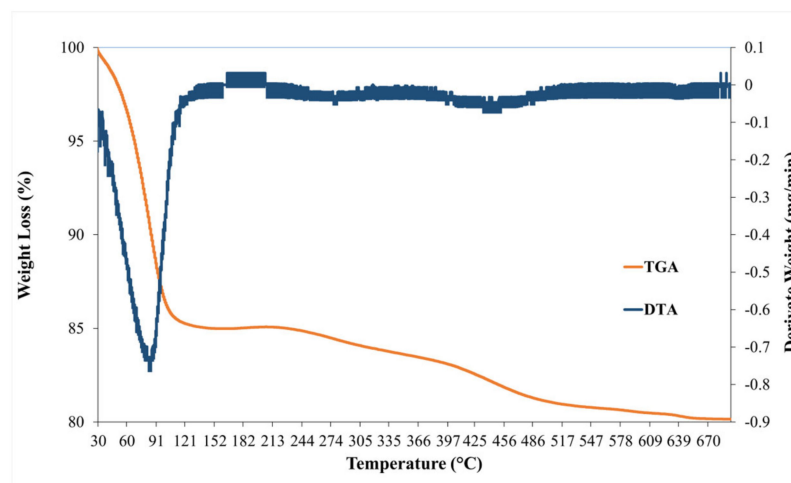

Figure 8. TGA and DTA curves of magnetite NCQDs.

3.8. Results of Magnetic Property Analysis

To verify the magnetic properties between the NCQDs and the magnetite NCQDs, an external magnet was utilized. The inset of Figure 9a shows easy separation of magnetite NCQDs but not NCQDs. Magnetite NCQDs are well-dispersed in water, and when an external magnet is applied, the magnetite particles will immediately attach to the magnet, which can improve the separation process. The magnetic properties of magnetite NCQDs play an important role if they are to be easily separated during environmental remediation. The saturation magnetization (Ms) value of magnetite NCQDs is 41.022 emug^{-1}, as shown

in Figure 9. Based on previous research, the saturation magnetization value was only 27 emug^{-1}, which is lower than the current study [23]. The higher saturation magnetization in the current study, double that of previous research, indicates improved magnetic properties. This enhancement suggests better magnetite loading, making the magnetite NCQDs more suitable for applications requiring strong magnetic responsiveness, such as targeted drug delivery or magnetic separation.
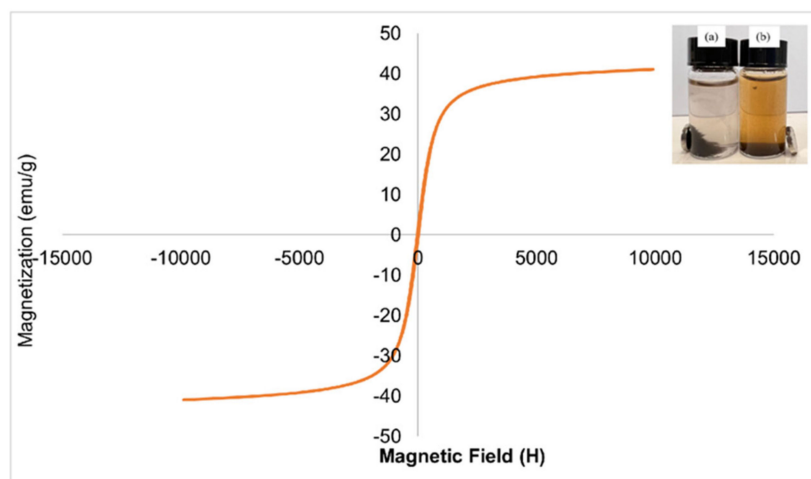

Figure 9. Magnetization curve of magnetite NCQDs with the inset showing the separation appearance of the adsorbent using an external magnet: (**a**) magnetite NCQDs and (**b**) NCQDs.

3.9. Study of the Adsorption Parameters

The selection of specific concentrations, dosages, and contact times was based on preliminary studies aimed at optimizing adsorption efficiency. An initial tramadol concentration of 10 mg/L was chosen to represent typical pharmaceutical pollutant levels in wastewater. The contact time for tramadol adsorption was determined by conducting experiments with varying durations, and the optimal contact time was identified when equilibrium was achieved. The adsorbent dosage was selected based on the relationship between tramadol removal efficiency and the adsorbent dosage, with the optimal dosage determined at the point where further increases in the dosage resulted in minimal improvement in removal efficiency. These parameters were chosen to ensure a balance between efficiency, practicality, and reproducibility of the results.

The adsorption efficiency of magnetite NCQDs for tramadol removal was found to be 85.9% within 40 min under optimal conditions, as shown in Figure 10. This efficiency is higher than the 72.5% reported for copper removal using magnetite composites under similar conditions in a previous study [24]. This suggests that magnetite NCQDs have superior adsorption capabilities, particularly for pharmaceutical pollutants like tramadol.

For photocatalytic degradation, magnetite NCQDs achieved 90.4% degradation of tramadol within 50 min, which is comparable to or better than the performance of conventional photocatalysts reported in the literature, which typically range from 70 to 85% for similar pollutants [25]. The recyclability of magnetite NCQDs was also remarkable, with a slight reduction in efficiency from 86% to 80.8% after five cycles, indicating excellent stability. This performance aligns with or surpasses that of other nanocomposite photocatalysts used for wastewater treatment [26].
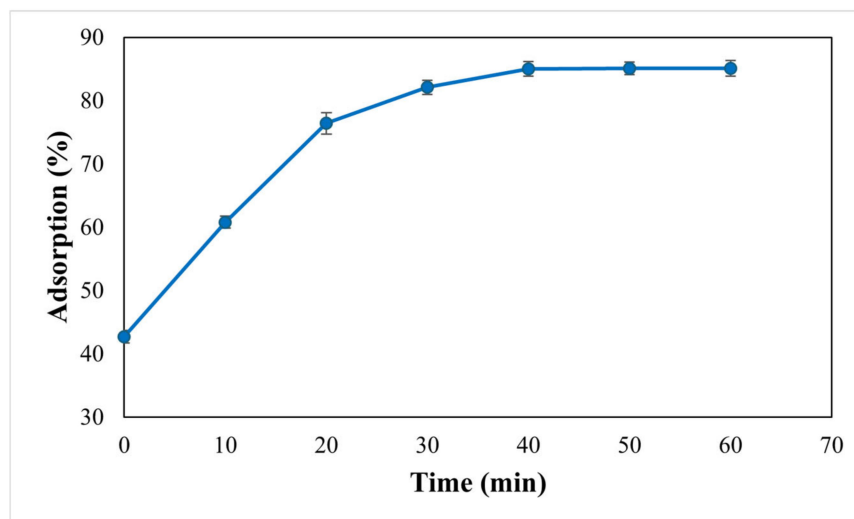
Figure 10. Percentage of tramadol adsorption by magnetite NCQDs at different time intervals.

The sorption mechanism in this study is primarily chemisorption, facilitated by interactions between tramadol molecules and functional groups (-OH, -COOH, -NH) on the magnetite NCQDs' surface. These interactions include hydrogen bonding, π-π interactions, and electrostatic forces, as confirmed through FTIR analysis. At pH 6.5, tramadol exists in its protonated form, carrying a positive charge, which is attracted to the negatively charged NCQDs, enhancing sorption efficiency. Compared to published studies, this research achieved 85.9% adsorption efficiency and 90.4% removal efficiency after photocatalysis, surpassing many methods reported in the literature. For instance, sodium-exchanged smectite clays demonstrated 65–70% adsorption efficiency for tramadol under optimized conditions, as highlighted in a recent study [25]. Additionally, a photo-Fenton-like system achieved 100% degradation for tramadol but required highly optimized experimental conditions [27]. The use of magnetite NCQDs, however, offers additional advantages, such as magnetic separation, reusability, and a combination of adsorption and photocatalysis, positioning this material as a promising solution for tramadol removal.

3.9.1. Impact of Contact Time

The result is shown in Figure 10. From the data, the rate of the adsorption increased rapidly from 0 to 40 min, and it reached an equilibrium state at around 40 min. The adsorption percentages increased drastically from 43.5% to 85.5% and gradually increased to 85.9%. Thus, 40 min could be considered a sufficient contact time for the adsorption of tramadol by magnetite NCQDs.

3.9.2. Impact of Adsorbent Dosage

Figure 11 shows the effect of different adsorbent dosages on the adsorption of tramadol. The graph reveals that the adsorption of tramadol increased rapidly with increasing dosages up to around 0.05 g. The highest adsorption percentage was observed at a dosage of 0.1 g, where the adsorption percentage was 90.84%. Further increasing the dosage above 0.05 g did not significantly improve the adsorption percentage. Therefore, 0.05 g of magnetite NCQDs could be suggested for this process. Currently, there are limited data available on the removal efficiency of tramadol using magnetite composites. Further research is needed to evaluate the potential of magnetite composites for pharmaceutical pollutant removal, including tramadol.
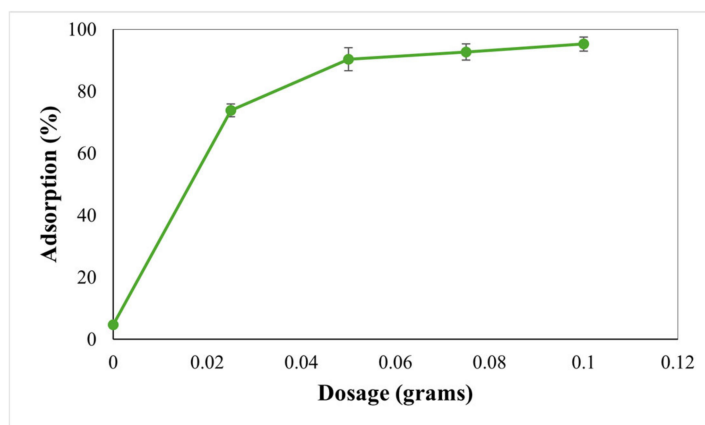
Figure 11. Percentage of tramadol adsorption by magnetite NCQDs at different adsorbent dosages.

3.9.3. Impact of Initial Concentration

The result is shown in Figure 12. The efficiency of tramadol removal by magnetite NCQDs was found to be dependent on the initial concentration of the tramadol solution. The maximum adsorption occurred at 2 mg L^{-1}, with a decrease in efficiency from 94.7% to 90.3% when the concentration increased up to 10 mg L^{-1}. The reduction in adsorption can be explained by the fact that the magnetite NCQDs' adsorbent surface has a limited number of binding sites. Once these sites are occupied, fewer interactions with additional molecules can occur, limiting further adsorption capacity.
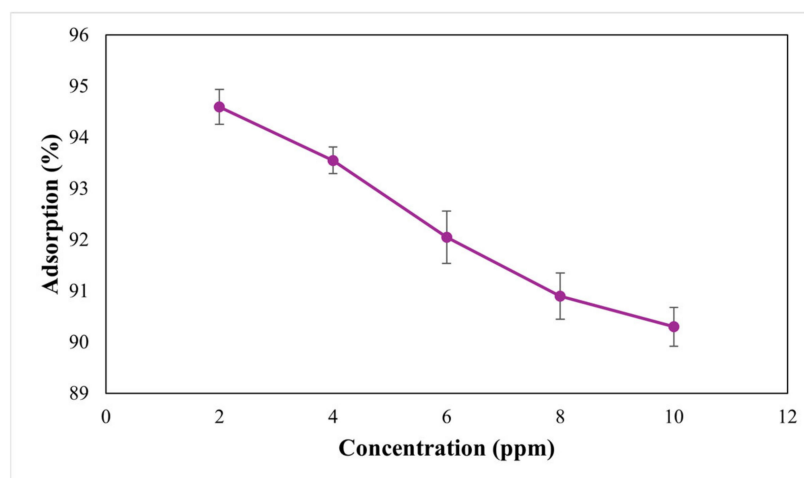

Figure 12. Percentage of tramadol adsorption by magnetite NCQDs at different initial concentrations.

3.9.4. Investigating the Contact Time of Photocatalytic Degradation

A tramadol solution of 10 mg/L was prepared, and 0.05 g of magnetite NCQDs was added. The process involved two stages, adsorption in the dark for 40 min and allowing tramadol to bind to the NCQDs, which achieved tramadol removal of about 85.9%. This was followed by photocatalysis under visible light. Samples were taken at intervals, and the degradation rate was calculated by comparing each sample's concentration to the initial level. The optimal contact time was identified as 50 min, where degradation stabilized, as shown in Figure 13.
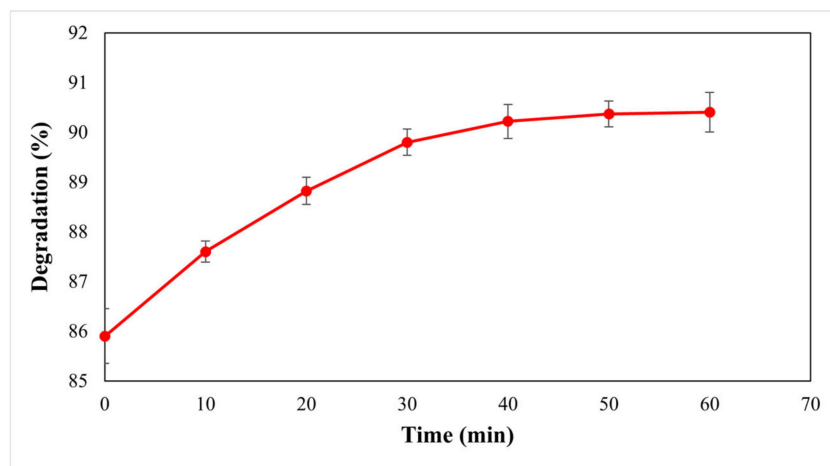
Figure 13. Photocatalytic degradation of tramadol solution by magnetite NCQDs at different time intervals.

From the data, the rate of photocatalytic degradation increases rapidly from 0 to 50 min, nearing equilibrium between 50 and 60 min. Tramadol removal increased drastically from 85.9% to 90.2% and gradually reached equilibrium at around 90.4%. Thus, 50 min is considered sufficient for removing tramadol through the photocatalytic degradation process using magnetite NCQDs. This study demonstrated that the adsorption process can remove approximately 85.9% of the tramadol, with an additional 4.5% removed through photocatalysis.

3.9.5. Investigating the Adsorption of Tramadol onto Magnetite NCQDs: Kinetics and Mechanism Analysis

The adsorption kinetics of tramadol by magnetite NCQDs were evaluated at 40 min of contact time using 0.05 g of adsorbent and a tramadol solution of 10 mg/L. The slope and intercept of straight line plots of $\log (Q_e - Q_t)\ vs\ t$, shown in Figure 14, gave the values of k_1 (in min^{-1}) and Q_e (in mg g^{-1}), respectively, and the R squared value obtained is 0.9653, which is close to unity, indicating fitness of the pseudo-first-order model. The k_1 value obtained was 0.1147 min^{-1}.
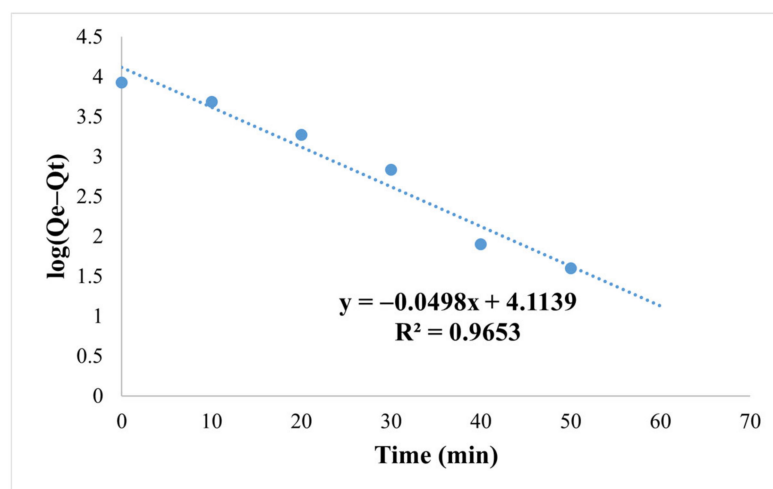

Figure 14. Pseudo-first-order kinetic plot.

The pseudo-second-order model was found to be more suitable for describing the adsorption kinetics of tramadol onto magnetite NCQDs than the pseudo-first-order model. This conclusion was drawn based on the high correlation coefficient of 0.996, as shown in

Figure 15. Therefore, it can be concluded that the adsorption process of tramadol onto magnetite NCQDs follows pseudo-second-order kinetics. The k_2 obtained was 0.00004 min^{-1}. The slow kinetics of tramadol adsorption onto the magnetite NCQDs is reasonable due to the large molecular size of tramadol.
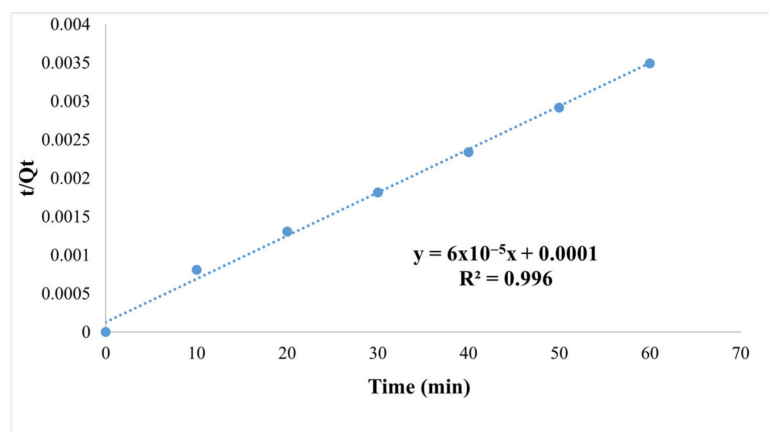

Figure 15. Pseudo-second-order kinetic plot.

Based on the k_1 and k_2 values, together with the R^2 values, the adsorption of tramadol onto the magnetite NCQDs is primarily driven by chemisorption rather than diffusion-controlled physical adsorption. Furthermore, the high regression coefficient for the pseudo-second-order kinetic model suggests the suitability of magnetite NCQDs for high adsorption of tramadol, possibly in a multilayered manner.

3.9.6. Investigating the Kinetics of Photocatalysis

The Langmuir–Hinshelwood (L-H) model, a first-order kinetics model [28], was used to assess the photocatalytic reaction kinetics of tramadol. To determine the apparent specific reaction rate (k), ln (Ao/At) versus time was plotted. The linearity of the graph indicates that the photocatalytic degradation of tramadol conforms to the first-order kinetics model. Figure 16a shows the linear plot of *ln (A_o/A_t)* versus time for the photocatalysis of tramadol in the presence of magnetite NCQDs, revealing a k value of 0.0306 min^{-1} and a correlation (R^2) of 0.9903. Conversely, Figure 16b depicts a k value of only 0.008 min^{-1}, with an R^2 value of 0.9941 in the absence of magnetite NCQDs. The k values imply that the rate of tramadol degradation is swifter in the presence of magnetite NCQDs, indicating that magnetite NCQDs potentially possess numerous active surface sites for photocatalytic degradation reactions, leading to rapid tramadol degradation. The existence of functional groups on the surface of magnetite NCQDs had the potential to amplify the number of sites available for photoreactions and facilitate electron transfer between the catalyst and tramadol molecules. The rapid electron transport of magnetite NCQDs could also boost their ability to degrade tramadol molecules when exposed to UV light. Moreover, the π-π bonds between magnetite NCQDs and the benzene rings of tramadol structures could aid in the adsorption of tramadol molecules onto the NCQDs' surfaces, resulting in improved photocatalytic degradation activity. Magnetite NCQDs are capable of absorbing light in the UV-Vis to near-infrared range, enabling the utilization of solar energy for photocatalysis. The photo-excitations in the NCQDs play a vital role in the oxidation and reduction reactions during photocatalytic degradation, making the magnetite NCQDs effective electron transporters and acceptors and thus ideal photocatalysts [29]. The presence of nitrogen atoms can improve the fluorescent properties of the NCQDs by inducing charge delocalization, while their atomic size and surface defects can enhance electronic conductivity and electron concentration, leading to improved photo-excitation

performance [30]. Moreover, the nanoscale size of the NCQDs promotes charge transport and enhances electronic conductivity, making them effective electron acceptors and donors that facilitate electron transfer in the reaction system.
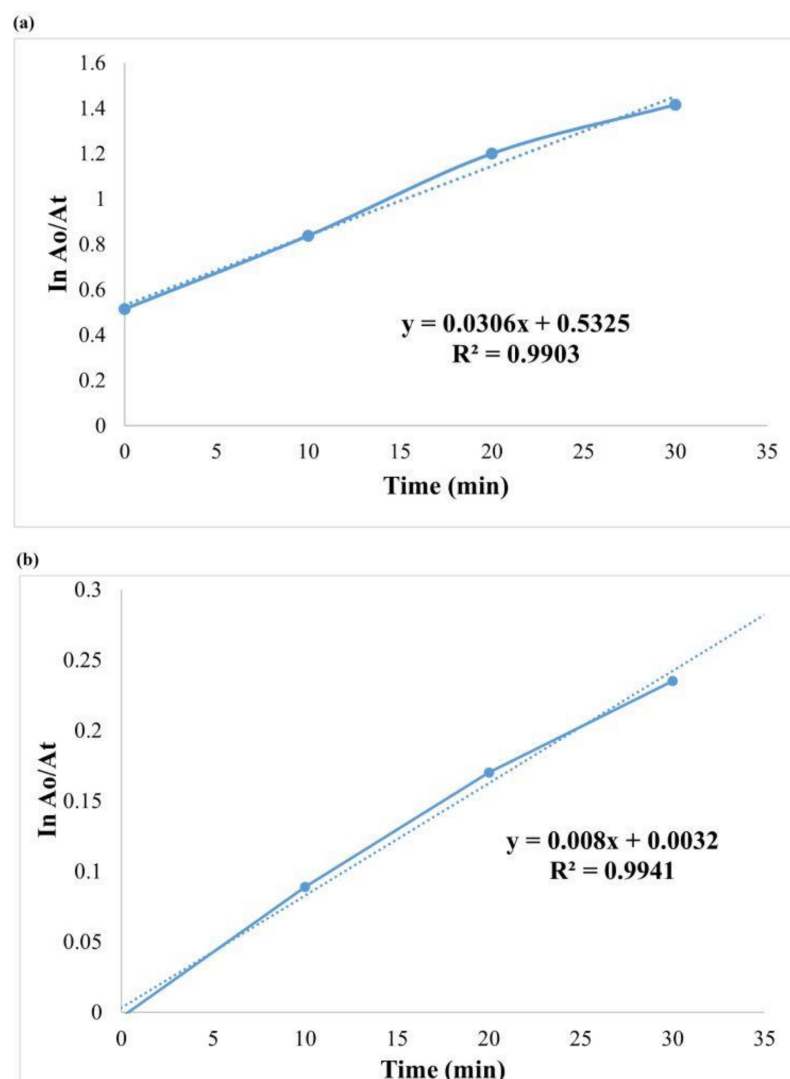

Figure 16. Graph of $ln(A_0/A_t)$ versus time for the photocatalytic degradation of tramadol, showing first-order kinetics in (**a**) the presence and (**b**) the absence of magnetite NCQDs.

During the photocatalytic degradation process, a first-order kinetics model was utilized to evaluate the photodegradation rate using Equation (6), where k is the reaction rate constant.

Figure 17a shows the linear plot of $ln(1/[A_t])$ versus time for the photocatalysis of tramadol in the presence of magnetite NCQDs, revealing a rate constant (k) of $0.0098\,min^{-1}$ and a correlation coefficient (R^2) of 0.9181. Figure 17b illustrates the photocatalysis in the absence of magnetite NCQDs, with a k value of $0.1779\,min^{-1}$ and $R^2 = 0.8891$.

In brief, the photocatalysis of tramadol using magnetite NCQDs fits well with first-order kinetics. From the photocatalysis of tramadol solution, the degradation of tramadol was reported to be around 25% and 85% in the absence and presence of magnetite NCQDs, respectively. The degradation rate of tramadol decreases when the tramadol is consumed during photocatalysis.
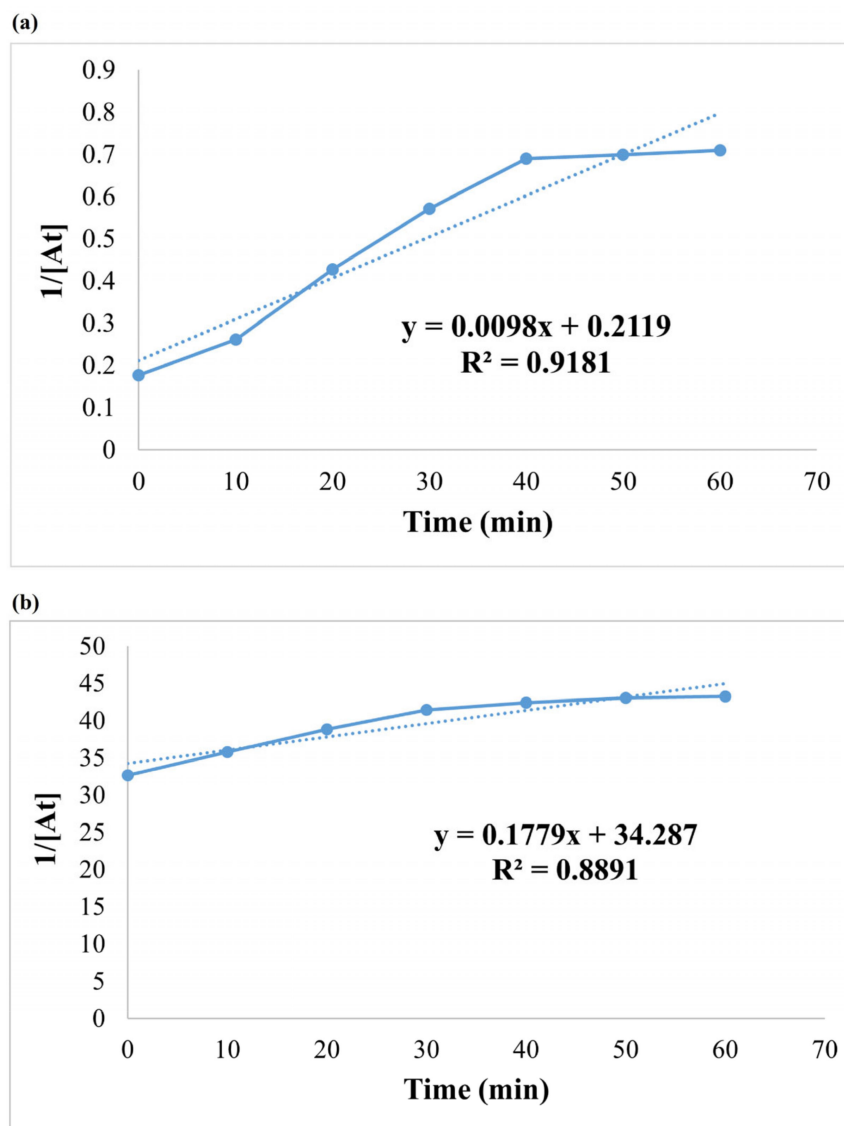
(a)

$$y = 0.0098x + 0.2119$$
$$R^2 = 0.9181$$

(b)

$$y = 0.1779x + 34.287$$
$$R^2 = 0.8891$$

Figure 17. Graphs (1/[A] versus time) of the photocatalytic degradation of tramadol, showing second-order kinetics in (**a**) the presence and (**b**) the absence of magnetite NCQDs.

3.9.7. Recyclability of Magnetic NCQDs

Magnetite NCQDs act as the adsorbent and the photocatalyst in removing tramadol in wastewater treatment plants through adsorption and photocatalysis. After the adsorption and photocatalysis, the magnetite NCQDs are easily separated from the aqueous solution using the external magnet. In order to be considered eco-friendly, the magnetite NCQDs were evaluated for their recyclability [31]. The removal efficiency slightly dropped from 86% to 80.8% after five successive cycles, as shown in Figure 18. The desorption of tramadol was conducted at pH 1 by using 0.1M of HCl in continuous shaking mode in order to remove the tramadol from the surface of magnetite NCQDs. During the fifth cycle, the tramadol removal efficiency from the spent adsorbent dropped to approximately 80%. Above five cycles of usage, the magnetite NCQDs led to tramadol removal below 80%. Thus, the current study limited the recyclability of the magnetite NCQDs to only five to ensure effective removal efficiency.
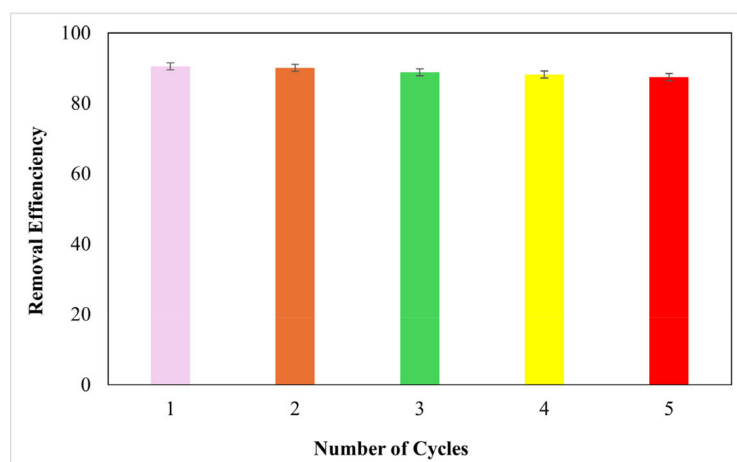
Figure 18. Recyclability of magnetite NCQDs in tramadol solution removal.

4. Conclusions

Magnetite NCQDs with strong magnetic properties were synthesized from eco-friendly empty fruit bunches (EFBs) through hydrothermal treatment and co-precipitation, utilizing lignin as the source material. These superparamagnetic NCQDs, with an average particle size of 13.53 nm, were successfully functionalized and demonstrated excellent performance as adsorbents and photocatalysts by efficiently separating photo-generated electron–hole pairs and minimizing surface charge recombination.

The batch adsorption experiments revealed that magnetite NCQDs rapidly removed tramadol from aqueous solutions, achieving an adsorption efficiency of 85.9% within 40 min under optimal conditions. The adsorption data were well-fitted by the Freundlich model ($R^2 = 0.996$), and the kinetics analysis indicated that the pseudo-second-order model better described the adsorption process compared to the pseudo-first-order model.

Under UV light, magnetite NCQDs achieved a tramadol degradation efficiency of 90.4% within 50 min, compared to 85.9% in their absence, highlighting their significant photocatalytic activity. Additionally, the magnetite NCQDs exhibited remarkable stability, retaining high photocatalytic efficiency even after five cycles of use.

Author Contributions: Conceptualization, L.Y.N. and C.Y.N.; data curation, A.K.M.C. and K.J.N.; formal analysis, L.Y.N., A.K.M.C. and K.J.N.; funding acquisition, L.Y.N. and C.Y.N.; investigation, K.J.N.; methodology, L.Y.N., C.Y.N. and K.J.N.; project administration, L.Y.N. and C.Y.N.; resources, L.Y.N.; supervision, L.Y.N. and C.Y.N.; validation, A.K.M.C. and K.J.N.; visualization, L.Y.N., A.K.M.C. and K.J.N.; writing—original draft, L.Y.N. and K.J.N.; writing—review and editing, E.M., Y.P.L. and M.M.B.-A. All authors have read and agreed to the published version of the manuscript.

Data Availability Statement: The original contributions presented in this study are included in the article. Further inquiries can be directed to the corresponding authors.

Conflicts of Interest: The authors declare no conflicts of interest.

References

1. Antonopoulou, M.; Thoma, A.; Konstantinou, F.; Vlastos, D.; Hela, D. Assessing the Human Risk and the Environmental Fate of Pharmaceutical Tramadol. *Sci. Total Environ.* **2020**, *710*, 135396. [CrossRef]
2. Cao, J.; Hu, Y.; Chen, L.; Xu, J.; Chen, Z. Nitrogen-Doped Carbon Quantum Dot/Graphene Hybrid Nanocomposite as an Efficient Catalyst Support for the Oxygen Reduction Reaction. *Int. J. Hydrog. Energy* **2017**, *42*, 2931–2942. [CrossRef]
3. Dong, Z.; Qi, J.; Yue, L.; Zhou, H.; Chen, L.; Gu, J.; He, Y.; Wu, H. Biomass-Based Carbon Quantum Dots and Their Agricultural Applications. *Plant Stress.* **2024**, *11*, 100411. [CrossRef]

4.   Tadesse, A.; RamaDevi, D.; Hagos, M.; Battu, G.; Basavaiah, K. Synthesis of Nitrogen Doped Carbon Quantum Dots/Magnetite Nanocomposites for Efficient Removal of Methyl Blue Dye Pollutant from Contaminated Water. *RSC Adv.* **2018**, *8*, 8528–8536. [CrossRef]

5.   Jamaludin, N.; Tan, T.L.; Zaman, A.S.; Sadrolhosseini, A.R.; Rashid, S.A. Acid-Free Hydrothermal-Extraction and Molecular Structure of Carbon Quantum Dots Derived from Empty Fruit Bunch Biochar. *Materials* **2020**, *13*, 3356. [CrossRef]

6.   Derman, E.; Abdulla, R.; Marbawi, H.; Sabullah, M.K. Oil Palm Empty Fruit Bunches as a Promising Feedstock for Bioethanol Production in Malaysia. *Renew. Energy* **2018**, *129*, 285–298. [CrossRef]

7.   Ng, L.Y.; Wong, T.J.; Ng, C.Y.; Amelia, C.K.M. A Review on Cellulose Nanocrystals Production and Characterization Methods from Elaeis Guineensis Empty Fruit Bunches. *Arab. J. Chem.* **2021**, *14*, 103339. [CrossRef]

8.   Zhang, J.; Lin, S.; Han, M.; Su, Q.; Xia, L.; Hui, Z. Adsorption Properties of Magnetic Magnetite Nanoparticle for Coexistent Cr(VI) and Cu(II) in Mixed Solution. *Water* **2020**, *12*, 446. [CrossRef]

9.   Rani, U.A.; Ng, L.Y.; Ng, C.Y.; Mahmoudi, E.; Ng, Y.-S.; Mohammad, A.W. Sustainable Production of Nitrogen-Doped Carbon Quantum Dots for Photocatalytic Degradation of Methylene Blue and Malachite Green. *J. Water Process Eng.* **2021**, *40*, 101816. [CrossRef]

10.   Latip, N.A.; Sofian, A.H.; Ali, M.F.; Ismail, S.N.; Idris, D.M.N.D. Structural and Morphological Studies on Alkaline Pre-Treatment of Oil Palm Empty Fruit Bunch (OPEFB) Fiber for Composite Production. *Mater. Today Proc.* **2019**, *17*, 1105–1111. [CrossRef]

11.   Zhao, X.; Liu, Y.; Lv, Y.; Liu, M. Research on Lignin-Modified Flexible Polyurethane Foam and Its Application in Sound Absorption. *J. Ind. Eng. Chem.* **2024**, *137*, 327–337. [CrossRef]

12.   Moussout, H.; Ahlafi, H.; Aazza, M.; Maghat, H. Critical of Linear and Nonlinear Equations of Pseudo-First Order and Pseudo-Second Order Kinetic Models. *Karbala Int. J. Mod. Sci.* **2018**, *4*, 244–254. [CrossRef]

13.   Suno, M.; Ichihara, H.; Ishino, T.; Yamamoto, K.; Yoshizaki, Y. Photostability Studies on (±)-TRAmadol in a Liquid Formulation. *J. Pharm. Health Care Sci.* **2015**, *1*, 5. [CrossRef]

14.   Tran, H.D.; Nguyen, D.Q.; Do, P.T.; Tran, U.N.P. Kinetics of Photocatalytic Degradation of Organic Compounds: A Mini-Review and New Approach. *RSC Adv.* **2023**, *13*, 16915–16925. [CrossRef]

15.   Chen, X.; Hossain, M.F.; Duan, C.; Lu, J.; Tsang, Y.F.; Islam, M.S.; Zhou, Y. Isotherm Models for Adsorption of Heavy Metals from Water—A Review. *Chemosphere* **2022**, *307*, 135545. [CrossRef]

16.   Ngwu, C.; Nnaji, J.; Odoemelam, S. Characterization of Magnetite and Zinc Oxide Nanoparticles Bio-Synthesized with Snakeweed (Stachytarpheta Indica). *Tech. Rom. J. Appl. Sci. Technol.* **2020**, *2*, 49–61. [CrossRef]

17.   Talib, L.; Ali, A.K.; Hussein, A.G. Preparation and Characterization of Au Quantum Dots Using Laser in Benzene and Study of the Pulse Energy Effect on Quantum Size. *Int. J. Nanoelectron. Mater.* **2023**, *16*, 891–904.

18.   Wu, S.; Wang, X.; Zhu, Y.; He, P.; Yu, X.; Qin, F.; Yao, Y.; Ren, L. Different Types of Nitrogen-Doped CQDs Loaded by CoP Used as OER Electrocatalysts. *Inorg. Chem. Commun.* **2023**, *153*, 110872. [CrossRef]

19.   Sunny, A.; Thirumurugan, A.; Balasubramanian, K. Laser Induced Fano Scattering, Electron-Phonon Coupling, Bond Length and Phonon Lifetime Changes in α-Fe$_2$O$_3$ Nanostructures. *Phys. Chem. Chem. Phys.* **2020**, *22*, 2001–2009. [CrossRef]

20.   Kim, T.; Jin, X.; Song, J.H.; Jeong, S.; Park, T. Efficiency Limit of Colloidal Quantum Dot Solar Cells: Effect of Optical Interference on Active Layer Absorption. *ACS Energy Lett.* **2020**, *5*, 248. [CrossRef]

21.   Ognjanović, M.; Bošković, M.; Kolev, H.; Dojčinović, B.; Vranješ-Đurić, S.; Antić, B. Synthesis, Surface Modification and Magnetic Properties Analysis of Heat-Generating Cobalt-Substituted Magnetite Nanoparticles. *Nanomaterials* **2024**, *14*, 782. [CrossRef] [PubMed]

22.   Dorniani, D.; Hussein, M.; Kura, A.; Fakurazi, S.; Shaari, A.; Ahmad, Z. Sustained Release of Prindopril Erbumine from Its Chitosan-Coated Magnetic Nanoparticles for Biomedical Applications. *Int. J. Mol. Sci.* **2013**, *14*, 23639–23653. [CrossRef] [PubMed]

23.   Winsett, J.; Moilanen, A.; Paudel, K.; Kamali, S.; Ding, K.; Cribb, W.; Seifu, D.; Neupane, S. Quantitative Determination of Magnetite and Maghemite in Iron Oxide Nanoparticles Using Mössbauer Spectroscopy. *SN Appl. Sci.* **2019**, *1*, 1636. [CrossRef]

24.   Shahrashoub, M.; Bakhtiari, S. The Efficiency of Activated Carbon/Magnetite Nanoparticles Composites in Copper Removal: Industrial Waste Recovery, Green Synthesis, Characterization, and Adsorption-Desorption Studies. *Microporous Mesoporous Mater.* **2021**, *311*, 110692. [CrossRef]

25.   Haciane, Y.M.; Bouafia, S.C.; Chabani, M.; Benramdan, I.K.; Mebtouche, M.; Neffa, M.; Touzani, R. Optimization and Modeling of Tramadol Hydrochloride Degradation by the Homogenous Photo-Fenton-like System Assisted by in Situ H$_2$O$_2$ Formation. *Water Sci. Technol.* **2023**, *87*, 1174–1186. [CrossRef]

26.   Zheng, Z.; He, J.; Zhang, Z.; Kumar, A.; Khan, M.; Lung, C.W.; Lo, I.M.C. Magnetically Recyclable Nanophotocatalysts in Photocatalysis-Involving Processes for Organic Pollutant Removal from Wastewater: Current Status and Perspectives. *Environ. Sci. Nano* **2024**, *11*, 1784–1816. [CrossRef]

27.   Thiebault, T.; Guégan, R.; Boussafir, M. Adsorption Mechanisms of Emerging Micro-Pollutants with a Clay Mineral: Case of Tramadol and Doxepine Pharmaceutical Products. *J. Colloid. Interface Sci.* **2015**, *453*, 1–8. [CrossRef]

28. Asenjo, N.G.; Santamaría, R.; Blanco, C.; Granda, M.; Álvarez, P.; Menéndez, R. Correct Use of the Langmuir–Hinshelwood Equation for Proving the Absence of a Synergy Effect in the Photocatalytic Degradation of Phenol on a Suspended Mixture of Titania and Activated Carbon. *Carbon. N. Y.* **2013**, *55*, 62–69. [CrossRef]
29. Mandal, S.K.; Paul, S.; Datta, S.; Jana, D. Nitrogenated CQD Decorated ZnO Nanorods towards Rapid Photodegradation of Rhodamine B: A Combined Experimental and Theoretical Approach. *Appl. Surf. Sci.* **2021**, *563*, 150315. [CrossRef]
30. Liu, Y.; Jiang, L.; Li, B.; Fan, X.; Wang, W.; Liu, P.; Xu, S.; Luo, X. Nitrogen Doped Carbon Dots: Mechanism Investigation and Their Application for Label Free CA125 Analysis. *J. Mater. Chem. B* **2019**, *7*, 3053–3058. [CrossRef]
31. Agustin, M.B.; Lehtonen, M.; Kemell, M.; Lahtinen, P.; Oliaei, E.; Mikkonen, K.S. Lignin Nanoparticle-Decorated Nanocellulose Cryogels as Adsorbents for Pharmaceutical Pollutants. *J. Environ. Manag.* **2023**, *330*, 117210. [CrossRef]